Available online at www.sciencedirect.com
ScienceDirect
Physics Letters B 660 (2008) 161–166
PHYSICS LETTERS B
www.elsevier.com/locate/physletb

Neutron–proton analyzing power at 12 MeV and inconsistencies in parametrizations of nucleon–nucleon data

R.T. Braun [a,b], W. Tornow [a,b,*], C.R. Howell [a,b], D.E. González Trotter [a,b], C.D. Roper [a,b], F. Salinas [a,b], H.R. Setze [a,b], R.L. Walter [a,b], G.J. Weisel [c]

[a] *Department of Physics, Duke University, Durham, NC 27708-0308, USA*
[b] *Triangle Universities Nuclear Laboratory, Durham, NC 27708-0308, USA*
[c] *Department of Physics, Penn State Altoona, Altoona, PA 16601, USA*

Received 10 August 2007; received in revised form 6 December 2007; accepted 29 December 2007

Available online 4 January 2008

Editor: D.F. Geesaman

Abstract

We present the most accurate and complete data set for the analyzing power $A_y(\theta)$ in neutron–proton scattering. The experimental data were corrected for the effects of multiple scattering, both in the center detector and in the neutron detectors. The final data at $E_n = 12.0$ MeV deviate considerably from the predictions of nucleon–nucleon phase-shift analyses and potential models. The impact of the new data on the value of the charged pion–nucleon coupling constant is discussed in a model study.

PACS: 13.75.Cs; 24.70.+s; 25.40.Dn

1. Introduction

There are reasons why low-energy ($E_N \leqslant 20$ MeV) nucleon–nucleon (NN) scattering data might appear to be of limited use in constraining NN phase-shift analyses (PSAs) [1,2] and potential models (PMs) [3–7]. For one thing, the deuteron bound-state properties already provide a fairly stringent constraint for any NN PM, and might seem sufficient. For another, low-energy scattering data can provide constraints only for the lower partial wave NN interactions and, even then, cannot determine individual partial waves. For example, the low-energy analyzing power, $A_y(\theta)$, is governed by the three angular momentum $L = 1$ interactions, ${}^3P_0$, ${}^3P_1$, and ${}^3P_2$. Although NN data provide constraints on the ${}^3P$ phase shifts taken together, it cannot determine each parameter unambiguously [8].

Despite the very small magnitude of NN $A_y(\theta)$, its importance derives from the fact that it is possible experimentally to measure such data to great precision. As a result, NN $A_y(\theta)$ can provide a crucial test of our understanding of the NN interaction and of the nuclear force in general.

Perhaps the most important controversy surrounding current NN interaction models concerns the pion–nucleon coupling constant, $g_\pi^2/4\pi$. In Ref. [9], Machleidt and Slaus point out that low-energy proton–proton (p–p) $A_y(\theta)$ data are very sensitive to the neutral pion–nucleon coupling constant, implying a value of $g_{\pi^0}^2/4\pi \leqslant 13.4$ (see also Ref. [10]). At the same time, the correct description of the quadrupole moment of the deuteron and low-energy neutron–proton (n–p) $A_y(\theta)$ data requires meson-exchange based NN potential models to have values for the neutral and charged pion–nucleon coupling constants $g_{\pi^0}^2/4\pi$ and $g_{\pi^\pm}^2/4\pi$, respectively, of 14.0 or larger. The latter finding is clearly inconsistent with the results of the Nijmegen group's NI93 PSA ($g_{\pi^0}^2/4\pi = 13.47 \pm 0.11$ and $g_{\pi^\pm}^2/4\pi = 13.54 \pm 0.05$ [11]) and of the VPI group ($g_{\pi^0}^2/4\pi = 13.3$ and $g_{\pi^\pm}^2/4\pi = 13.9$ from NN scattering [12,13] and $g_{\pi^0}^2/4\pi = 13.75 \pm 0.15$ from $\pi^\pm p$ scattering [14]).

In principle, this inconsistency can be reduced by assuming a charge-splitting of the pion–nucleon coupling constant, i.e.,

* Corresponding author at: Department of Physics, Duke University, Durham, NC 27708-0308, USA.
E-mail address: tornow@tunl.duke.edu (W. Tornow).

0370-2693/$ – see front matter
doi:10.1016/j.physletb.2007.12.039

one could assume that the neutral pion couples to the nucleon with a different strength than the charged pion. In Refs. [9,10] it was shown that the combination of $g^2_{\pi^0}/4\pi = 13.6$ and $g^2_{\pi^\pm}/4\pi = 14.4$ creates a sufficiently large value for the quadrupole moment of the deuteron, and reproduces the low-energy p–p $^3P_0$ phase shifts.

At the same time that the analyses of Refs. [9,10] were performed, there were indications that n–p differential cross-section data at intermediate energies favored a larger value for $g^2_{\pi^\pm}/4\pi$. On this, see Ref. [15] for a comprehensive overview of recent determinations of $g^2_\pi/4\pi$ and especially Ref. [16], which quotes $g^2_{\pi^\pm}/4\pi = 14.50 \pm 0.26$ obtained from n–p differential cross-section data at $E_n = 162$ MeV. However, the recent n–p differential cross-section data obtained at IUCF at 194 MeV [17] do not support this larger value of $g^2_{\pi^\pm}/4\pi$.

Although it seems likely that there is no significant charge splitting in the pion–nucleon coupling constants at intermediate energies, the question remains unresolved at low energies. On the one hand, the theoretical models used to account for the charge dependence of the singlet NN scattering lengths, $^1S_0$, do not allow for any large charge splitting of $g^2_\pi/4\pi$. On the other hand, many low-energy data suggest a significant charge splitting. We report here on the results of a new n–p $A_y(\theta)$ experiment carried out at $E_n = 12.0$ MeV utilizing improved data-taking and data-analysis techniques. For references to previous n–p $A_y(\theta)$ measurements see Refs. [18–20]. Our results confirm the inconsistencies between low-energy analyzing power and available theoretical models of the NN interaction.

2. Experimental setup

The experimental setup is shown in Fig. 1. Polarized neutrons with mean energy of 12.0 MeV and total energy spread of about 400 keV were produced via the polarization-transfer reaction ^{2}H$(\vec{d},\vec{n})^3$He at 0°. The polarized deuteron beam was accelerated to $E_d = 9.40$ MeV and entered through a 4.6 μm Havar foil into a small (3.14 cm long, 0.48 cm radius) gas cell filled with 7.8 atm of deuterium gas and capped with a 0.1 cm thick gold beamstop. The gas cell was mounted inside a 1.8 m-thick wall made of concrete, paraffin, iron, copper, and lead, to shield the neutron detectors from the direct flux of the neutron source. Typical deuteron beam intensities on target were 1.5 μA and typical values for the deuteron vector polarization $|p_z|$ were 0.65. The polarized neutrons produced at 0° relative to the incident deuteron beam passed through a collimation system to produce a rectangular shaped neutron beam at the position of the proton-containing active target labeled "Center Detector" in Fig. 1. The center detector (CD) consisted of an upright cylinder made of the plastic scintillator material NE102A with dimensions 1.9 cm diameter and 3.8 cm height. The CD was located at a distance of 172 cm from the neutron source and was mounted via a short light guide onto a 5 cm diameter photomultiplier tube (PMT).

Neutrons scattered to the left or right were detected by five pairs of neutron detectors (NDs) positioned symmetrically relative to the incident neutron beam direction in the horizontal

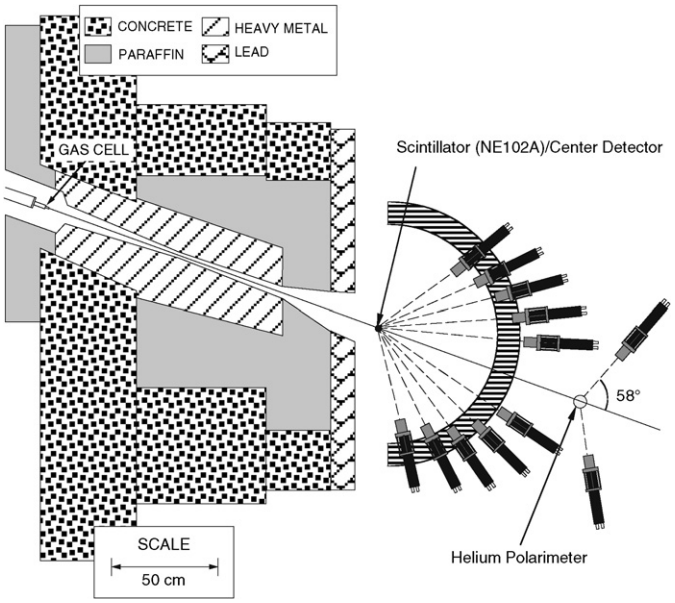

Fig. 1. Experimental setup for n–p $A_y(\theta)$ measurements in TUNL's shielded neutron source area.

scattering plane. The NDs were filled with the liquid scintillator material NE213. These detectors had excellent neutron-gamma pulse-shape discrimination capabilities and had an active volume of 4.3 cm wide, 11.9 cm high and 7.5 cm deep. They were viewed by 5 cm diameter PMTs through 0.5 cm thick Pyrex glass windows and 7.5 cm long light guides. The neutron detectors were mounted onto (low-mass) 30 cm high stands and placed on an aluminum ring surrounding the CD. The center-to-center distance between the CD and the neutron detectors ranged from 45 cm to 70 cm depending on scattering angle. The angular separation between the neutron detectors was 12° (lab). In order to cover the angular range from $\theta_{\rm lab} = 16°$ to 72° in 4° steps, three settings of the five detector pairs were required. The absolute magnitude of the neutron polarization was measured with a neutron polarimeter located downstream of the n–p scattering arrangement. The polarimeter consisted of a ^{4}He gas scintillator pressurized to 100 atm (95% He, 5% Xe) and a pair of neutron detectors positioned at $\theta_{\rm lab} = 58°$, which were identical to those used for n–p scattering. In order to reduce instrumental asymmetries for the n–p and n–^{4}He measurements, the deuteron vector polarization p_z, and therefore the neutron polarization, was flipped at a frequency of 10 Hz (between up and down relative to the horizontal scattering plane). The n–p and n–^{4}He data were accumulated simultaneously in six runs, each lasting about 250 data-taking hours.

The data-acquisition electronics recorded the center-detector pulse height (CDPH) in the CD, the neutron time of flight (NTOF) between the CD and the NDs, and spectra for each neutron detector displaying pulse-shape information. Since the energy of the scattered neutrons varied from $E_{n'} = 11.1$ MeV at $\theta_{\rm lab} = 16°$ to $E_{n'} = 1.1$ MeV at $\theta_{\rm lab} = 72°$, different hardware thresholds were used for the NDs. In addition, three different gains were used for the CD signals (using different dynodes).

Software cuts were set on the CDPH in the CD and the pulse height in the NDs to eliminate pulses at the extreme ends of

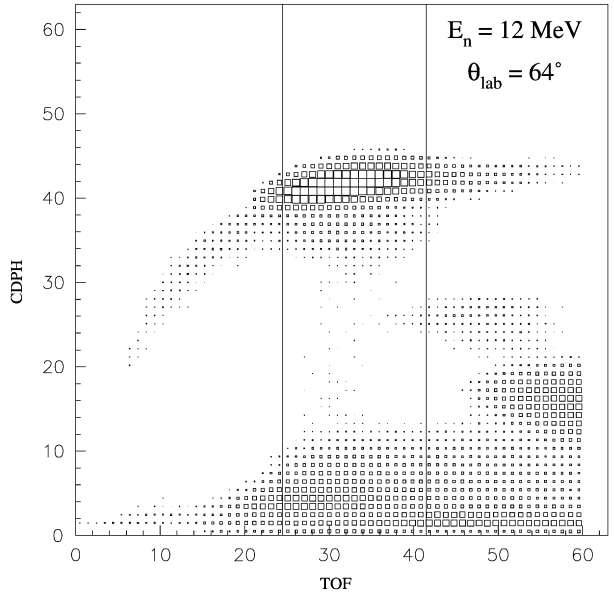

Fig. 2. 2D spectrum of compressed CDPH versus NTOF for scattering to $\theta_{\text{lab}} = 64°$. A tight NTOF gate was set around the elastic neutron peak in order to remove as many background events as possible.

the spectra. Gates were also set on the neutrons in the pulse-shape discrimination spectra and wide gates were set on the elastic peak of the NTOF spectrum. All four of these cuts (identical for spin-up and spin-down spectra) were used to generate two-dimensional (2D) spectra of CDPH versus NTOF, for scattering to the left and right NDs and for neutron spin up and spin down. An example of such a spectrum is shown in Fig. 2 where the CDPH scale has been temporarily compressed in order to fit within 64 channels. Tight NTOF gates were set in these 2D spectra eliminating the tails of the peak, as shown in Fig. 2, in order to identify the elastic scattering events of interest (again, identical for spin-up and spin-down spectra). These new NTOF gates were used to sort the final CDPH spectra (now in their full 512-channel resolution) corresponding to each neutron detector and spin state. The CDPH spectra were used to determine the n–p yields and scattering asymmetries, after applying the corrections described in the following section. The above process was also followed to sample the accidental (i.e., time uncorrelated) background by using an NTOF cut located at times shorter than the gamma peak. The accidental background proved to be extremely small.

3. Data analysis

After the sorting procedure described above and the subtraction of the accidental events, the data still contained a number of finite-geometry and multiple-scattering effects. To remove these effects, Monte Carlo calculations were performed to simulate the experiment. Two effects are due exclusively to the finite size of the center detector and the neutron detectors and have a slight effect on single-scattering events. First, because there is a range of angles subtended by each detector set at each nominal angle and because the cross section of n–p elastic scattering varies over this range, we must report an effective angle.

Table 1
Results of n–p $A_y(\theta)$ experiment at $E_n = 12.0$ MeV

$\theta_{\text{c.m.}}$	PDE correction	Final results
32.6	0.00014 ± 0.00016	0.00854 ± 0.00067
40.5	0.00004 ± 0.00016	0.01231 ± 0.00064
48.5	0.00006 ± 0.00015	0.01451 ± 0.00065
56.5	0.00013 ± 0.00013	0.01443 ± 0.00063
64.4	-0.00005 ± 0.00015	0.01560 ± 0.00063
72.4	0.00294 ± 0.00022	0.01659 ± 0.00067
80.5	-0.00185 ± 0.00014	0.01470 ± 0.00060
88.4	0.00019 ± 0.00017	0.01386 ± 0.00057
96.3	0.00072 ± 0.00018	0.01198 ± 0.00059
104.2	-0.00136 ± 0.00018	0.01110 ± 0.00058
112.2	-0.00114 ± 0.00028	0.00662 ± 0.00062
120.2	0.00108 ± 0.00029	0.00558 ± 0.00065
128.2	0.00103 ± 0.00021	0.00483 ± 0.00056
136.0	-0.00018 ± 0.00036	0.00372 ± 0.00067
143.8	-0.00029 ± 0.00040	0.00287 ± 0.00079

These were calculated by our code and are listed in the first column of Table 1. This effect is small; the largest shift is no more than a half of a degree. The second finite-geometry effect concerns the value of $A_y(\theta)$ itself, again due to the range of angles subtended by each neutron detector. Effective $A_y(\theta)$ values were calculated by our Monte Carlo code and these were compared to the values from the code's library. The ratio between these two values was then applied to the data. Once again, the correction is small; only the first four angles had corrections that were larger than the uncertainty of the calculation (about 0.00012).

In addition to elastic scattering, multiple scattering events occur in the CD. About 50% (depending on ND angle) of these events were eliminated as a result of the NTOF gate. Nevertheless, the CDPH spectrum contained multiple scattering events amounting to approximately 2% of all single scattering events. Our Monte Carlo simulation showed that the only significant processes were those due to double scattering, specifically neutron double scattering from hydrogen (^{1}H–^{1}H), neutron scattering from hydrogen and subsequent scattering from carbon (^{1}H–^{12}C), and neutron scattering from carbon and subsequent scattering from hydrogen (^{12}C–^{1}H). In performing these calculations, we used complete libraries of cross-section and polarization data for both n–^{1}H and n–^{12}C scattering. We will return to the subject of the n–^{12}C library in our discussion of the PDE correction.

We also removed edge-effect events from the data, which result when recoil protons leave the CD before depositing their full energy. Along with the double scattering events, these counts elongate the tails of the CDPH peak, especially to the left (low-energy) side.

A sample CDPH spectrum is shown in Fig. 3 (top panel). The solid curve represents our Monte Carlo simulation for a scattering angle of $\theta_{\text{lab}} = 36°$, while the small open circles show the experimental data. A greatly expanded view is shown in the middle panel, where the open circles again indicate the experimental data. The curve labeled "single" is the calculated single scattering contribution, normalized to the data. The curves labeled "double" are the double scattering contributions ^{1}H–^{1}H,

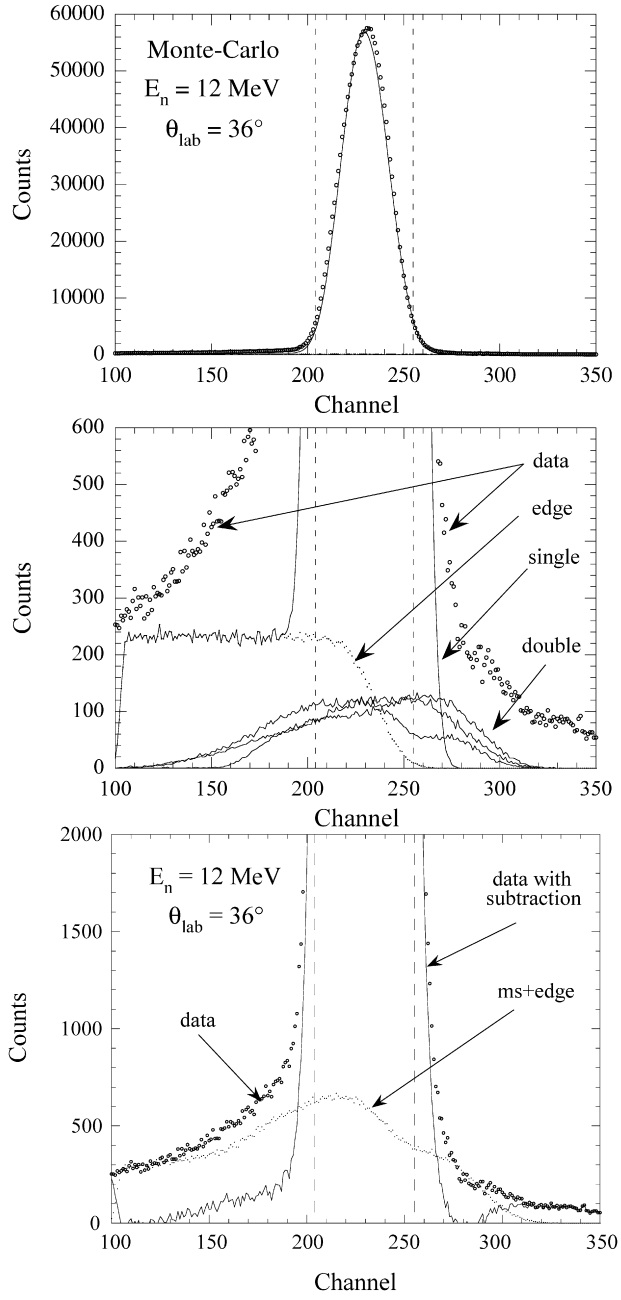

Fig. 3. The top panel shows a comparison of calculated (solid curve) and measured (dots) center-detector pulse height (CDPH) spectrum in the center detector for scattering to $\theta_{\rm lab} = 36°$. The middle panel shows an expanded view with focus on calculated multiple-scattering and edge effect contributions. The bottom panel shows an additional expanded view focusing on the remaining background. See text for details.

^{1}H–^{12}C, and ^{12}C–^{1}H. Finally, the dotted curve labeled "edge" is the calculated pulse-height distribution due to edge effects. As can be seen from a second expanded view, the bottom panel of Fig. 3, even after subtraction of all counts due to multiple scattering and edge effects (labeled "ms + edge"), a small background remains (amounting to about 0.3% of the single scattering events). A number of fits were used to estimate this remaining background, ranging from a linear fit between channel numbers 150 and 350 to a parabolic fit between channel numbers 180 and 280. Due to the smallness of the remaining background, the asymmetry proved to be independent of our background choice, within statistical uncertainties. We also concluded that the background was unpolarized. For all ND angle settings we approximated the remaining background by a linear function connecting the left and right sides of the CDPH peak (for example, in Fig. 3 from channel 180 to 280). The remaining background seen above channel 290 in the bottom panel of Fig. 3 is due to cross-talk effects between two adjacent detectors, specifically neutron scattering from the detector positioned at a larger scattering angle (and shorter distance from the CD) to the detector of interest.

Three sets of gates were used to calculate the yields and asymmetries, at 10% (shown in Fig. 3 by the dashed lines), 30%, and 50% of the CDPH peak maximum. In Fig. 3, this is done for $N_L^{\uparrow}$, for spin up scattering to the left ND at $\theta_{\rm lab} = 36°$. Similarly, the yields $N_R^{\uparrow}$, $N_L^{\downarrow}$, and $N_R^{\downarrow}$ were obtained to calculate the asymmetry $\epsilon = (\alpha - 1)/(\alpha + 1)$ with $\alpha = \sqrt{\frac{N_L^{\uparrow}}{N_R^{\uparrow}} \frac{N_R^{\downarrow}}{N_L^{\downarrow}}}$. The nominal gates were the 30% set. The other two gates (the 10% and 50% set) were used to check on the appropriateness of the background subtraction. Within statistical uncertainty, the results for ϵ proved to be independent of the choice of the gate width.

In order to extract the n–p $A_y(\theta)$ from the measured asymmetry $\epsilon(\theta)$, the neutron polarization p_y^n must be known. For this purpose the n–^{4}He asymmetry data acquired with the neutron polarimeter referred to above were processed and analyzed in the same way as the n–p asymmetry data. In this case the ^{4}He recoil pulse height in the high-pressure gas scintillator plays the role of the CDPH in the plastic scintillator used for the n–p asymmetry measurements. The neutron polarization was obtained from $\epsilon_{\rm He}(58°) = (\alpha_{\rm He} - 1)/(\alpha_{\rm He} + 1) = \bar{A}_y(58°) p_y^n$, where $\alpha_{\rm He}$ is defined as above. Here, the effective analyzing power $\bar{A}_y(58°)$ for n–^{4}He scattering at $E_n = 12.0$ MeV was calculated for the present neutron polarimeter geometry via Monte Carlo calculations. The n–^{4}He phase shifts of Stammbach and Walter [21] were used. All of the relevant multiple scattering processes were included. We obtained $\bar{A}_y(58°) = -0.554 \pm 0.008$, where the uncertainty is mainly of a systematic nature reflecting the uncertainty associated with the n–^{4}He phase shifts. The average neutron polarization was $p_y^n = 0.563 \pm 0.008$.

At such a high level of precision, a subtle systematic effect comes into play, which does not cancel by reversal of the neutron polarization. This is the polarization dependent efficiency (PDE) [19] of the neutron detectors. The NDs contain hydrogen and carbon in the ratio of 1.21:1. The double scattering process ^{12}C–^{1}H in the NDs, which accounts for about 10% of the total neutron detection efficiency, is sensitive to the n–^{12}C $A_y(\theta)$. If the n–^{12}C $A_y(\theta)$ is not constant over the range of neutron energies $E_{n'}$ seen by a particular ND, an instrumental asymmetry will occur. Typical values for $\Delta E_{n'}$ are 800 keV. A realistic correction for this effect requires a detailed knowledge of the n–^{12}C $A_y(\theta)$, especially in the resonance region of the n–^{12}C total cross section between 2.0 and 8.5 MeV neutron energy. In

this energy regime the n–^{12}C $A_y(\theta)$ changes rapidly and therefore causes sizeable PDE effects.

All of the post-1985 n–p $A_y(\theta)$ measurements have been corrected for the PDE. However, due to the lack of a detailed n–^{12}C $A_y(\theta)$ database, especially at low energies, the accuracy of the associated corrections was limited. In assembling our data library, we used the thirty-three n–^{12}C $A_y(\theta)$ angular distributions measured by Roper et al. [22] in the energy range from 2.2 to 8.5 MeV. From $E_n = 0$ to 6.5 MeV, we used an R-matrix analysis by Hale [23], which included the data from Ref. [22]. In certain regions (especially for forward angles and for neutron energies between 3.5 and 4.5 MeV), the analysis of Ref. [23] missed the $A_y(\theta)$ data slightly and we therefore substituted Legendre polynomial fits to the data of Ref. [22] in these regions. Between 6.5 MeV and 8.5 MeV, we used fits to the data of Ref. [22] as well as the recent phase-shift analysis (PSA) of Chen and Tornow [24]. Above $E_n = 8.5$ MeV, we used the Chen–Tornow PSA exclusively. The new data by Roper et al. and the analyses of Hale, Chen and Tornow improved the n–^{12}C $A_y(\theta)$ database considerably, making corrections for the PDE more reliable.

We ran our Monte Carlo code for 20 separate legs, each leg of three million events, and each leg starting from a different random number. The PDE correction to the $A_y(\theta)$ data was taken as the difference between the $A_y(\theta)$ result with polarization effects turned on in the neutron detectors and the result with the polarization turned off. The second column of Table 1 lists our final PDE corrections. Note that they vary greatly from one data point to the other due to the pronounced resonance features in n–^{12}C scattering at low energy. It is important also to note that our present results agree well with the overall trend of the PDE corrections of Ref. [20], which used a different Monte Carlo code and a different database. Our reason for having much greater confidence in the present PDE results is due to our extensive and detailed work in revising the data libraries, as outlined above.

The third column in Table 1 summarizes our final results for $A_y(\theta)$ in n–p scattering at $E_n = 12.0$ MeV. Note the small overall uncertainty. The final results include uncertainties in $A_y(\theta)$ due to statistics, the measurement of beam polarization, the multiple-scattering calculation, the PDE calculation, and the remaining background (typically zero) all added in quadrature. The final uncertainties are about half of those of the previous TUNL n–p $A_y(\theta)$ measurement at $E_n = 12.0$ MeV [20]. This is partly due to the fact that the atomic beam polarized ion source used in the present study produced about four times the deuteron current as the Lamb–Shift source used in the previous study.

4. Discussion

Fig. 4 shows the present n–p $A_y(\theta)$ in comparison to the NN phase-shift analysis prediction (solid curve) of the Nijmegen group, NI93. Clearly, NI93 provides a larger $A_y(\theta)$ throughout the entire angular distribution. The accuracy of the neutron polarization determined in the present work does not allow for a renormalization of the $A_y(\theta)$ data beyond the error bars given in Fig. 4. Furthermore, the present n–p $A_y(\theta)$ data are in good agreement with the trend established by previous TUNL data where a different method was used for determining p_y^n [20].

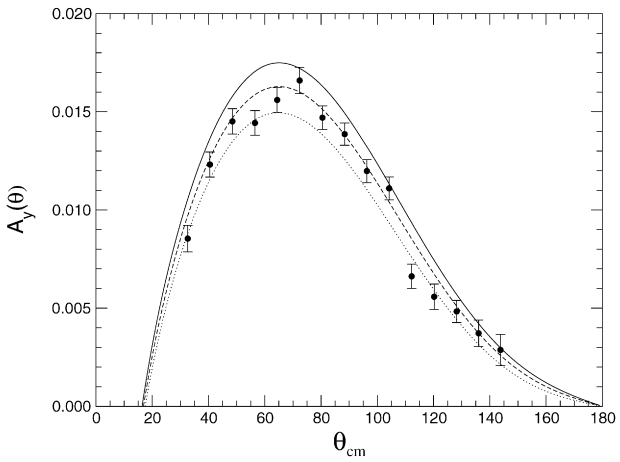

Fig. 4. Neutron–proton $A_y(\theta)$ data at $E_n = 12.0$ MeV in comparison to theoretical predictions. The error bars associated with the data represent the overall uncertainty of the data with statistical and systematic uncertainties added in quadrature. The solid curve is the Nijmegen NI93 PSA prediction. The other curves are for the CD-Bonn based model study which varies the charged pion coupling constant. Here, for $g^2_{\pi^0}/4\pi$, all three curves use 13.6. For $g^2_{\pi^\pm}/4\pi$, the calculation using 13.6 coincides on this scale with the Nijmegen NI93 PSA result (solid curve); the dashed curve uses 14.0 and the dotted curve 14.4.

As we have pointed out in the introduction, the underlying NN dynamics that characterize $A_y(\theta)$ precludes us from extracting unambiguous information about the ^3P_j NN interactions. However, we can conclude that the NI93 NN PSA overestimates the n–p $A_y(\theta)$ at $E_n = 12.0$ MeV. This statement is of considerable importance considering the fact that most NN potential model builders use the NI93 PSA results or the associated database for determining the free parameters of their models. One has to conclude that all the recent so-called high-precision NN potential models overestimate the n–p $A_y(\theta)$ at low energies. This observation has far-reaching consequences for nuclear scattering systems with $A > 2$, which are much more sensitive to the ^3P_j NN interactions than the NN system [25].

Valuable information can be obtained from the present data if they are compared to variations of the theoretical predictions. Here we focus on the charged pion coupling constant [9,10]. Fig. 4 shows our data in comparison to three theoretical predictions based on the CD-Bonn NN potential, which use three different values of the charged pion–nucleon coupling constant, $g^2_{\pi^\pm}/4\pi$. In these three models, only the S-wave NN interactions of CD-Bonn were refitted. All three predictions use the same neutral pion coupling constant, $g^2_{\pi^0}/4\pi = 13.6$. The curve using $g^2_{\pi^\pm}/4\pi = 13.6$ is indistinguishable on this scale from the prediction of NI93 (solid curve). The dashed curve in Fig. 4 uses $g^2_{\pi^\pm}/4\pi = 14.0$ and the dotted curve uses $g^2_{\pi^\pm}/4\pi = 14.4$. The values of χ^2 per degree of freedom associated with the solid, dashed and dotted curves are 6.0, 1.7, and 2.5, respectively. Therefore, this model study confirms and puts on more solid ground the findings of Refs. [9,10] regarding low-energy

n–p $A_y(\theta)$ data and their demand for a charge splitting of $g_\pi^2/4\pi$.

In summary, the present data represent the most accurate and complete n–p $A_y(\theta)$ angular distribution ever reported. Our model study based on the CD-Bonn NN potential model strongly supports a substantial charge dependence of the pion–nucleon coupling constant. Our results are inconsistent with the existing global NN PSAs of the Nijmegen [11] and VPI [12,13] groups and with high-precision NN potential models. However, our results agree with inconsistencies previously noticed between data and predictions for the ${}^3S_1$–${}^3D_1$ mixing parameter ϵ_1 in n–p scattering at low energies [26] and also with requirements placed on the charged coupling constant by the quadrupole moment of the deuteron [9]. Of course, it is possible that neither of these scenarios is the "correct" one. Perhaps the impasse comes because we are at the point where the precision of our data and the development of our "low energy" theoretical models has pushed the paradigm of meson-exchange based NN potential models beyond its limits.

Acknowledgements

This work was supported in part by the US Department of Energy, Office of Nuclear Physics, under Grant No. DE-FG02-97ER41033. The authors would like to thank R. Machleidt for valuable contributions to this work.

References

[1] V.G.J. Stoks, R.A.M. Klomp, M.C.M. Rentmeester, J.J. de Swart, Phys. Rev. C 48 (1993) 792.
[2] R. Arndt, W.J. Briscoe, I.I. Strakovsky, R.L. Workman, SAID program, http://gwdac.phys.gwu.edu.
[3] V.G.J. Stoks, R.A.M. Klomp, C.P.F. Terheggen, J.J. de Swart, Phys. Rev. C 49 (1994) 2950.
[4] R.B. Wiringa, V.G.J. Stoks, R. Schiavilla, Phys. Rev. C 51 (1995) 38.
[5] R. Machleidt, F. Sammarruca, Y. Song, Phys. Rev. C 53 (1996) R1483.
[6] D.R. Entem, R. Machleidt, Phys. Rev. C 68 (2003) 041001.
[7] E. Epelbaum, W. Glöckle, U.G. Meissner, Nucl. Phys. A 747 (2005) 362.
[8] T. Tornow, W. Tornow, Few-Body Syst. 26 (1999) 1.
[9] R. Machleidt, I. Slaus, J. Phys. G 27 (2001) R69.
[10] R. Machleidt, in: Proc. Workshop on Critical Issues in the Determination of the Pion–Nucleon Coupling Constant, Uppsala, 1999, Phys. Scr. T 87 (2000) 47.
[11] V. Stoks, R. Timmermans, J.J. de Swart, Phys. Rev. C 47 (1993) 512.
[12] R.A. Arndt, I.I. Strakovsky, R.L. Workman, Phys. Rev. C 50 (1994) 2731.
[13] R.A. Arndt, I.I. Strakovsky, R.L. Workman, Phys. Rev. C 52 (1995) 2246.
[14] R.A. Arndt, R.L. Workman, M.M. Pavan, Phys. Rev. C 49 (1994) 2729.
[15] J. Blomgren (Ed.), Proc. Workshop on Critical Issues in the Determination of the Pion–Nucleon Coupling Constant, Uppsala, 1999, Phys. Scr. T 87 (2000) 1.
[16] J. Rahm, et al., Phys. Rev. C 57 (1998) 1077.
[17] M. Sarsour, et al., Phys. Rev. Lett. 94 (2005) 082303.
[18] W. Tornow, C.R. Howell, M.L. Roberts, P.D. Felsher, Z.M. Chen, R.L. Walter, G. Mertens, I. Slaus, Phys. Rev. C 37 (1988) 2326, and references therein.
[19] D. Holslin, J. McAninich, P.A. Quin, W. Haeberli, Phys. Rev. Lett. 61 (1988) 1561.
[20] G.J. Weisel, W. Tornow, C.R. Howell, P.D. Felsher, M. AlOhali, Z.P. Chen, R.L. Walter, J.M. Lambert, P.A. Treado, I. Slaus, Phys. Rev. C 46 (1992) 1599.
[21] Th. Stammbach, R.L. Walter, Nucl. Phys. A 180 (1972) 225.
[22] C.D. Roper, et al., Phys. Rev. C 72 (2005) 024605.
[23] G.M. Hale, private communication, 2000.
[24] Z.P. Chen, W. Tornow, J. Phys. G: Nucl. Part. Phys. 31 (2005) 1249.
[25] W. Tornow, H. Witala, A. Kievsky, Phys. Rev. C 57 (1998) 555.
[26] W. Tornow, C.R. Gould, D.G. Hasse, J.R. Walston, Phys. Rev. C 65 (2002) 047002.